Developing Martini Coarse-Grained Nitrogen Gas Model for Lipid Nanobubble Simulations

Fujia Tian[1,2,#], Xubo Lin[1,#,*]

1. Institute of Single Cell Engineering, Key Laboratory of Ministry of Education for Biomechanics and Mechanobiology, Beijing Advanced Innovation Center for Biomedical Engineering, School of Biological Science and Medical Engineering, Beihang University, Beijing 100191, China.
2. Current Affiliation: Department of Physics, City University of Hong Kong, Hong Kong 999077, China.

* Correspondence to: linxbseu@buaa.edu.cn (XL).

# These authors contribute equally to this work.

The authors declare no competing financial interest.

Abstract

Lipid nanobubbles have shown a great potential to be used for the ultrasound molecular imaging and biocompatible drug and gene delivery carriers, which integrate the advantages of both the biocompatibility of lipids and potent physicochemical properties of nanobubbles. Molecular dynamics (MD) simulation provides a powerful tool to investigate fundamental scientific problems related to lipid nanobubbles. With coarse-grained models, the system can be simulated with longer time scale and larger length scale. However, there are very few coarse-grained gas models for lipid nanobubble simulations. Hence, in this work, we developed a simple coarse-grained nitrogen gas model within Martini force field by adjusting the Lennard-Jones interactions of N_2 with itself, water, lipids, which well reproduced the density of pure N_2, the density of N_2 within nanobubbles, and the partitioning thermodynamics of N_2 in DPPC bilayers. Further lipid nanobubble self-assembly simulation validated the reliability of our coarse-grained N_2 parameters. Using three-component lipid nanobubbles consisting of 1,2-dipalmitoyl-sn-glycero-3-phosphocholine (DPPC), 1,2-dilinoleoyl-sn-glycero-3-phosphocholine (DUPC), and cholesterol, our coarse-grained MD simulations indicated that single-layer membranes could also have clear phase separation, the degree of which was proportional to the radius (r) of the lipid nanobubble, and reached the maximum when $r \to \infty$ (the planar lipid bi-monolayer at the gas-water interface). Besides, by comparing the planar lipid bi-monolayer (at gas-water interface) and lipid bilayer systems, we found that the latter had much less obvious phase separation. In short, our coarse-grained MD simulations using systems of lipid nanobubbles, lipid bi-monolayers and lipid bilayers will provide useful insights into the role of membrane curvature and interleaflet coupling in the phase separation of multi-component lipid membranes.

Keywords: Coarse-Grained Gas Model; Martini Force Field; Molecular Dynamics Simulations; Lipid Nanobubbles.

Introduction

Nanobubbles have many unique physicochemical properties and are reported to have better stability than microbubbles[1-2], which show great potential in a series of biomedical applications including ultrasound molecular imaging[3-4], drug/gene delivery[5-6], water treatment[7-8], sonoimmunotherapy[9], and so on. Amphiphilic molecules such as lipids can self-assemble along the air-water interface of nanobubbles. Similar to roles of pulmonary surfactant[10], these molecules can greatly reduce the surface tension of the interface and increase the stability of nanobubbles. As the most abundant component of cell membrane, lipids play vital roles in maintaining its proper structure and functions. Hence, lipid nanobubbles may have excellent biocompatibility. On the other hand, lipid nanobubbles can fuse with cell membrane under a certain intensity of ultrasound[11]. Thus, cell membrane can incorporate lipids from lipid nanobubbles[11] and encapsulated gas molecules can re-distribute into the hydrophobic region of cell membrane[12]. The former will change the local membrane components, while the latter can decouple the two membrane leaflets and modify membrane structural properties. These two aspects may both dramatically affect the dynamics and functions of membrane proteins, which is so far largely unexplored. In other words, there is plenty of room in revealing the effects of lipid nanobubbles on structure and dynamics of membrane proteins on molecular level, which may greatly expand current biomedical applications of lipid nanobubbles.

Molecular dynamics (MD) simulations provide a powerful tool to investigate the interactions between biomolecules at atomic/near-atomic resolution[13]. Many computational efforts have been made to study the stability and dynamics of lipid nanobubbles as well as their interactions with model cell membrane[11, 14-16]. Especially, coarse-grained models (e.g. Martini[17-19]) allow MD simulations with much larger length scale and longer time scale than all-atom models, and thus can better capture the complexity of realistic lipid nanobubbles and cell membrane. However, in the current state-of-art coarse-grained MD simulations, gas molecules are modeled as the vacuum in the isothermal-isochoric (NVT) ensemble[11, 20-22]. This will greatly hinder precise studies on the interactions between lipid nanobubbles and model cell membrane. For one hand, in NVT ensemble, the lateral dimension is fixed, which makes the description of the large membrane deformation unreasonable. For the other hand, gas molecules can permeate into the hydrophobic region of lipid bilayer[12], the replacement of gas molecules with the vacuum could leave possible potent physical effects of these gas molecules on membrane lipids and proteins unclear. Hence, it will be critical to develop coarse-grained models of gas molecules for more precise description of the molecular-level interactions between lipid nanobubbles and biological systems (**Fig. 1**).

In this work, based on previous available results of N_2 gas from atomistic MD simulations[12, 23] and experiments[24-25] (main reason for the choice of N_2 gas), we developed MARTINI-compatible coarse-grained model of N_2 gas (**Fig. 1**), which can well reproduce the lipid nanobubble self-assembly process and overcome possible artifacts of lipid monolayer (e.g. lipid nanobubble[11], pulmonary surfactant[22], tear film[26]) simulations due to the vacuum treatment of gas molecules simultaneously. With this model, we performed coarse-grained MD simulations of lipid nanobubbles with three different lipid components, and found that obvious liquid-liquid phase separation could appear. Besides, by comparing with lipid bi-monolayer and lipid bilayer systems,

our results indicated that membrane curvature and interleaflet coupling could both have a strong impact on the phase separation of lipid membrane.

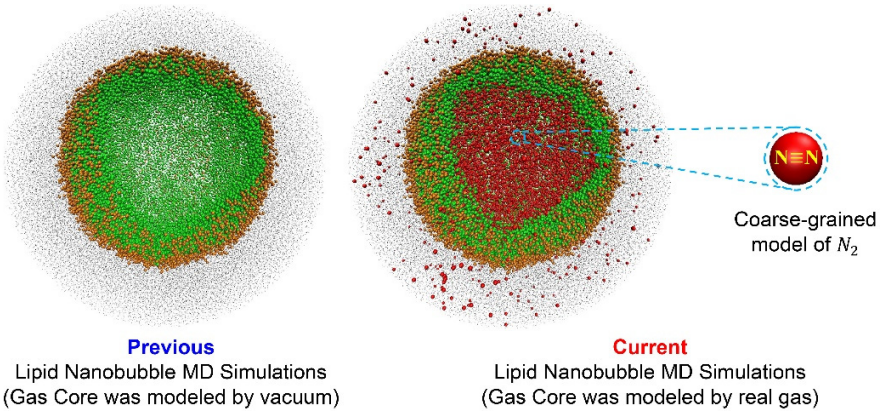

Figure 1. Coarse-grained gas (N_2) model makes the coarse-grained MD simulations of gas-water interfaces (e.g. lipid nanobubble) more realistic.

Model and Methods

In this work, coarse-grained parametrization of N_2 gas within Martini force field is mainly based on reproducing N_2 gas density (1.091 g/L)[24] at body temperature (~310K), atomistic simulations of N_2 nanobubbles[23] and N_2-lipid membrane interaction systems[12]. The obtained coarse-grained N_2 gas model was further validated in lipid nanobubble self-assembly simulations, which needs to be consistent with the experiments[4, 27]. Then, coarse-grained MD simulations of lipid nanobubble, lipid bi-monolayer and lipid bilayer systems with the optimized N_2 gas parameters were performed to reveal effects of membrane curvature and inter-leaflet coupling on the membrane phase separation.

Martini Force Field. As a popular coarse-grained model, Martini force field (version 2.1)[17-18] was used in the current work. In this model, generally 4 heavy atoms are mapped into 1 interaction site (For aromatic compounds, 2 or 3 to 1 mapping rule is applied.), including four main types: polar (P), nonpolar (N), apolar (C), and charged (Q). Four different subtypes (d=donor, a=acceptor, da=both, 0=none) are introduced to bead typed of N and Q to allow fine representation of the chemical nature. For bead types of P and C, five different subtypes (from 1, low polarity to 5, high polarity) are used to describe the degree of polarity. 10 levels of nonbonded interactions using different parameters (ε, σ) for Lennard-Jones (LJ) 12-6 potential energy function ($U_{LJ} = 4\varepsilon\left[\left(\frac{\sigma}{r}\right)^{12} - \left(\frac{\sigma}{r}\right)^{6}\right]$) are employed to describe the differential nonbonded interactions between different beads (**Table S1**). In this work, one new coarse-grained bead (G1) was used to represent one N_2 gas molecule. For Martini DPPC/DUPC lipids (DPPC: 1,2-dipalmitoyl-sn-glycero-3-phosphocholine, DUPC: 1,2-dilinoleoyl-sn-glycero-3-phosphocholine), the head-group consists of two charged beads (Q0, +1e and Qa, -1e), the glycerol ester backbone is represented by two nonpolar beads (Na), and each tail contains four apolar beads (C1, C1/C4). Five different beads (SP1, SC3, SC1, SC1, C1) parameterize cholesterol (Chol) molecules. A polar bead (P4) represents

one CG water. Systematic parameterization of the nonbonded interactions between G1 and these beads (lipids and water) was performed to reproduce the key physiochemical properties mentioned above.

Molecular Dynamics Simulations. The coarse-grained MD simulations of all systems were performed using GROMACS program v2016.5[28] and Martini force field[17-18], while the visualization of system snapshots was done using VMD[29]. For all simulations, periodic boundary conditions were applied in three dimensions. The v-rescale thermostat[30] with a relaxation time τ = 1 *ps* were used to maintain a constant temperature of 310K and a constant pressure of 1 bar was kept by Parrinello-Rahman pressure coupling[31] (Coupling constant is 5 *ps* and compressibility is 5×10^{-5} bar^{-1}.) in the NPT ensemble. For systems of pure N_2 gas, N_2-water and lipid nanobubbles, isotropic pressure coupling method was used. Meanwhile, semi-isotropic pressure coupling was applied to planar lipid bi-monolayer and lipid bilayer systems. A standard 1.2 nm cutoff was applied for van der Waals interactions, where the LJ potential was shifted to zero smoothly from 0.9 to 1.2 nm to reduce the cutoff noise. For columbic potential, a 1.2 nm cutoff was used for short-range electrostatic interactions while shifting to zero from 0 to 1.2 nm smoothly. The neighbor list for nonbonded interactions was updated every 10 steps with a cut-off of 1.2 nm.

Trajectory Analysis. *Normalized Lateral Contacts of Unsaturated lipids*. We first obtained the total number of lateral contacts, N_{Ld}, among unsaturated lipids DUPC in the phase separated lipid nanobubbles, vesicles and monolayer; contact was defined based on a distance cutoff of 0.6 nm between any two CG beads of the specified lipid type. Then we normalized N_{Ld} by N_{pure}, the total number of lateral contacts in a pure bilayer of DUPC obtained from the last 200 ns trajectory of a 600 ns run. Hence, N_{pure} represents the maximum number of contacts of unsaturated lipids in a fluid bilayer at the same temperature. The normalized number of L_d lipid contacts ($N = N_{Ld}/N_{pure}$) was used as a proxy for quantifying relative domain size.

Cholesterol Preference. Cholesterol preference was determined based on the number of contacts (cutoff 0.6 nm) of cholesterol with saturated (N_s) and unsaturated lipids (N_us) as

$$\chi_\mathrm{s} = \frac{N_\mathrm{s}/n_\mathrm{s}}{N_\mathrm{s}/n_\mathrm{s} + N_\mathrm{us}/n_\mathrm{us}}, \chi_\mathrm{us} = \frac{N_\mathrm{us}/n_\mathrm{us}}{N_\mathrm{s}/n_\mathrm{s} + N_\mathrm{us}/n_\mathrm{us}}$$

where χ_s and χ_us are the fraction of cholesterol in contact with saturated and unsaturated lipids, and n_s and n_us are the total number of CG beads of saturated and unsaturated lipids, respectively.

Results and Discussion

Parametrization of the Nitrogen Gas Model in Martini Force Field. In order to determine the Martini-compatible parameters for coarse-grained N_2 gas molecules, we firstly calibrated self-interaction parameters between N_2 coarse-grained beads (G1) by reproducing the experimental N_2 gas density (1.091 g/L) at body temperature[24]. According to Cao's work on the parameterization of N_2 gas molecules within SAFT-γ force field[32], the LJ interaction parameters between N_2 gas molecules are σ=0.36 nm and ε=0.7 kJ/mol. In order to evaluate the transferability from SAFT-γ coarse-grained N_2 parameters to Martini coarse-grained N_2 parameters, the LJ interaction parameters $\sigma \in$[0.28, 0.44] (nm) ($\Delta\sigma$=0.02 nm) and $\varepsilon \in$[0.2, 2.6] (kJ/mol) ($\Delta\varepsilon$=0.1 kJ/mol) for nonbonded interactions between G1 beads are systematically

benchmarked for the pure N_2 gas systems containing 1728 N_2 gas (Initial simulation box size: 6×6×6 nm^3. The total number of simulation systems is 9×25=225.). Each simulation system was run for 50 ns at T=310 K, which added up to a total simulation time of 9×25×50 ns=11.25 μs. The density of N_2 gas molecules was evaluated over the last 20 ns trajectories as shown in **Fig. 2a**. Generally, stronger LJ interactions will induce larger N_2 gas density. And the gas density with σ=0.36 nm and ε=0.7 kJ/mol is 1.087 g/L, which is close to and still able to achieve the exact experimental N_2 gas density (**Fig. 2a**). Considering the value of energy parameter ε is especially critical to the nanobubble formation process, while the value of distance parameter σ is less sensitive to the assemble states of N_2 gas in this range, we finally chose σ=0.36 nm and $\varepsilon \in$[0.7, 1.9] kJ/mol, which will be further determined in the following nanobubble formation benchmark simulations.

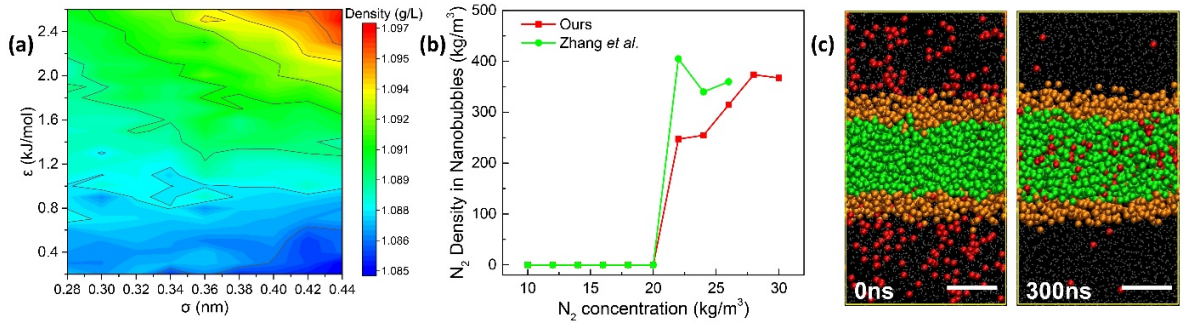

Figure 2. Coarse-grained Parameterization of Nitrogen Gas Molecules: **(a)** Density of nitrogen molecules calculated from the pure gas simulation systems at T = 310K with different σ ($\in$[0.28, 0.44]) and ε ($\in$[0.2, 2.6]) values. **(b)** Optimized parameters (ε is 1.6 and 1.4 kJ/mol for G1-G1 and G1-P4 LJ interactions respectively) enable better reproduction of the critical concentration for gas nucleation and gas density within the nanobubble in Zhang *et al.*'s work[23]. **(c)** Optimized parameters (ε is 1.4, 1.4, 1.7 and 2.0 kJ/mol for G1-Q0, G1-Qa, G1-Na and G1-C1 LJ interactions respectively) well reproduce the preferred localization of N_2 in DPPC lipid bilayer[12].

In order to obtain the nonbonded interaction parameters between coarse-grained N_2 beads (G1) and water beads (P4), Lorentz-Berthelot (LB) combination rule ($\sigma_{ij} = (\sigma_{ii} + \sigma_{ij})/2, \varepsilon_{ij}(T) = (1 - k_{ij})\sqrt{\varepsilon_{ii}(T)\varepsilon_{jj}(T)}$; k_{ij} is the scaling factor) was used. With the standard LB combination rule (k_{ij}=0, σ=0.42 nm and ε=1.9 kJ/mol for the nonbonded interactions between G1 and P4 beads), it is very difficult to reproduce the nanobubble formation process in water from the coarse-grained MD simulations (**Fig. S1**). However, this can be corrected by introducing a proper scaling factor k_{ij} for ε (**Tables S2**, **Fig. S1**). In other words, modified value of ε will be needed. Hence, LJ parameters σ=0.36 nm, $\varepsilon \in$[0.7, 1.9] kJ/mol for G1-G1 and σ=0.42 nm, $\varepsilon \in$[1.1, 2.0] kJ/mol for G1-P4 (**Table S3**) were carefully calibrated to obtain the optimized energy parameters which can well reproduce the critical N_2 gas concentration (22 kg/m^3) necessary for the nanobubble formation[23]. For each LJ parameter set (13×10=130 in total), the 50ns benchmark simulations (11 different initial gas concentrations from 10 kg/m^3 to 30 kg/m^3, Δ=2 kg/m^3, **Table S4**) were

performed. On average, 8 simulation systems of different initial gas concentrations were performed for each parameter set. In other words, the total simulation time for this part is 13×10×8×50 ns=52 μs. As shown in **Table S3**, LJ parameters of σ=0.36 nm, ε=1.6 kJ/mol for G1-G1 and σ=0.42 nm, ε=1.4 kJ/mol for G1-P4 enable the reproduction of the critical N_2 gas concentration for the nanobubble formation observed in all-atom MD simulations[23]. Using this parameter set, we could also obtain comparable the N_2 gas density within the nanobubble as Zhang *et al.*'s work[23] (**Fig. 2b**). It is worth mention that LJ parameters σ=0.36 nm, ε=1.6 kJ/mol for G1-G1 can also achieve the value of N_2 gas density (1.090 kg/m^3, **Fig. 2a**), which is closer to the experimental N_2 gas density at body temperature (1.091 kg/m^3). Hence, the interaction parameters for N_2-N_2 (G1-G1) and N_2-water (G1-P4) are fixed.

In order to expand the usage of Martini N_2 coarse-grained model to lipid systems, we further determined the LJ interaction parameters between N_2 bead (G1) and lipid coarse-grained beads. The benchmark simulations are mainly based on the united-atom MD simulations of N_2-DPPC lipid bilayer systems[12]. In this work, Li *et al.*[12] quantitatively described the partitioning thermodynamics of N_2 gas molecules into the hydrophobic regions of DPPC lipid bilayer. For our benchmark simulation systems, N_2 gas molecules (G1 bead) were initially evenly distributed in bulk water (P4 bead) region of the DPPC (Q0, Qa, Na, C1 beads) bilayer system. According to Martini interaction parameters (**Table S1**), Q0 and Qa share almost the same ε as P4 interacting with other beads. Hence, the ε values for G1-Q0 and G1-Qa nonbonded interactions are also fixed as 1.4 kJ/mol. Besides, the corresponding σ values for G1-Q0 and G1-Qa are 0.49 nm, while for G1-C1 and G1-Na give 0.42nm based on LB combination rule (the effective size of $\sigma = 0.47$ nm is assumed except charged and most apolar beads share $\sigma = 0.62$ nm). According to the nonbonded interaction rules for beads with different polarities in Martini coarse-grained model (**Table S1**), $\varepsilon \in$[1.6, 2.0] kJ/mol for G1-C1 and $\varepsilon \in$[1.4, 2.0] kJ/mol for G1-Na LJ interactions (**Table S5**) were finally evaluated in order to reproduce the distribution of N_2 gas molecules in the DPPC bilayer systems as indicated by united-atom MD simulations[12]. The energy parameter ε of G1-C1 nonbonded interaction should always be larger than that of G1-Na nonbonded interaction. Therefore, a total of 42 different sets of ε values were tested for G1-C1 and G1-Na interactions (**Table S5**). For each parameter set, four lipid bilayer systems with N_2 gas molecules of different numbers dispersed in bulk waters were performed. The simulation time of each benchmark system was 300 ns, with the last 100 ns used for the analysis of density profiles. Hence, the total simulation time for this part is 42×4×300 ns=50.4 μs. We finally chose ε=2.0 kJ/mol for G1-C1 and ε=1.7 kJ/mol for G1-Na, which properly reproduced the preferred localization of N_2 gas molecules (**Fig. S2**)[12]. Besides, we further obtained the nonbonded interactions parameters between N_2 gas molecules (G1 bead) and DUPC, cholesterol (C4, SP1, SC1 and SC3 beads) based on the above benchmark simulations and parameterization rules for nonbonded interactions in Martini model (**Table 1**).

Table 1. Finalized nonbonded Interaction Parameters of N_2 Gas Molecules and Main CG Sites in Martini FF.

Cross-term	σ (nm)	ε (kJ/mol)	Attractive term	Repulsive term

G1-G1	0.36	1.6	1.3931E-02	3.0326E-05
G1-P4	0.42	1.4	3.0739E-02	1.6873E-04
G1-Q0	0.49	1.4	7.7511E-02	1.0729E-03
G1-Qa	0.49	1.4	7.7511E-02	1.0729E-03
G1-Na	0.42	1.7	3.7325E-02	2.0488E-04
G1-C1	0.42	2.0	4.3912E-02	2.4104E-04
G1-C4	0.42	1.9	4.1717E-02	2.2898E-04
G1-SP1	0.40	1.7	2.7853E-02	1.1409E-04
G1-SC1	0.40	2.0	3.2768E-02	1.3422E-04
G1-SC3	0.40	2.0	3.2768E-02	1.3422E-04

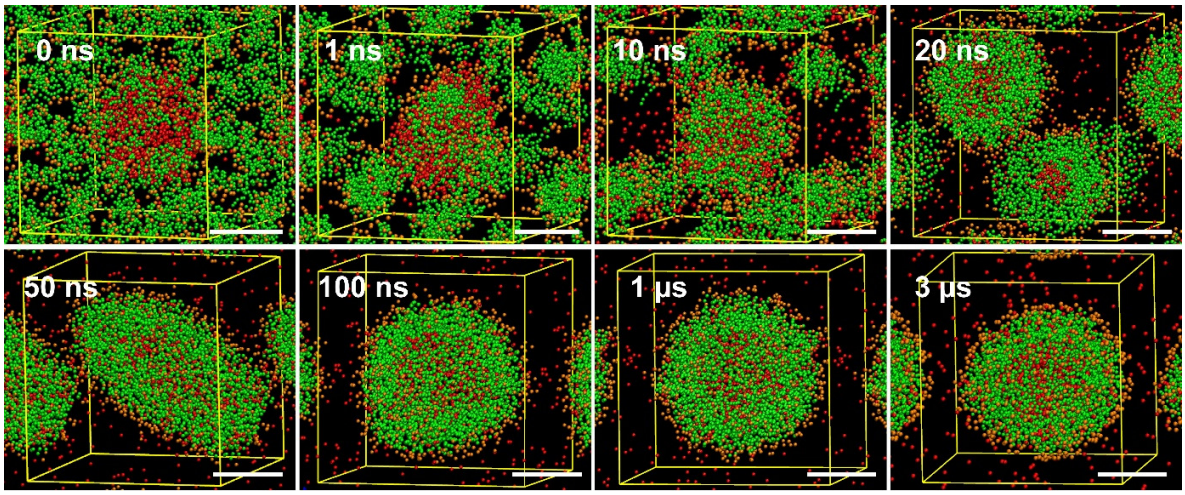

Figure 3. Self-assembly MD Simulations of Lipid Nanobubbles: 256 DPPC molecules were initially randomly distributed around a N_2 nanobubble (876 molecules), and gradually self-assembled into a single-layer lipid nanobubble with N_2 gas core inside and lipid head groups exposed outside. DPPC head groups are colored in orange, DPPC tails in green. Water molecules are not shown for clarity. Scale bar: 3 nm.

Lipid Nanobubble Self-Assembly Simulations Further Validated the Obtained Nitrogen Gas Coarse-grained Model. As we know, the lung alveoli provides the key air-water interface for the gas exchange process. The synthetic lipid lamellar bodies and surfactant proteins can be transported to the interface and re-assemble into the lipid monolayer structure[10, 22, 33]. Hence, from the perspective of bionics, the generation of gas bubbles in lipid solution can be one simple experimental method to synthesize lipid micro/nano- bubbles[4, 34-35]. In other words, the feasibility of the above-obtained N_2 gas coarse-grained model can be further evaluated by the lipid nanobubble self-assembly simulations. In order for this, we set up the initial simulation systems as follows: (1) N_2 gas nanobubble, who owns varying radius and number of molecules, was placed at the center of the simulation box (12×12×12 nm^3). (2) 180 or 256 DPPC molecules were evenly dispersed in other spaces except the gas nanobubble. (3) The whole system was then solvated by water molecules. In total, 12 self-assembly simulation systems (**Table S6**) were set up. During the

pre-equilibrium stage of each simulation, the position of N_2 gas molecules was constrained, while DPPC and water molecules were fully relaxed. Then, the simulation went through the subsequent 3 μs production run. For amphiphilic molecules such as DPPC lipids, it is easy to form micelles in water solution[36], which is possible to be converted into spherical vesicles in the absence of gas bubbles[37-38]. However, when the hydrophobic N_2 gas nanobubble existed, dispersed lipids or small lipid clusters could re-assemble along the gas-water interface with hydrophobic lipid tail toward the gas core, and thus form the lipid nanobubble. **Fig. 3** shows a typical assembly process for the lipid nanobubble formation in our simulations. First, small lipid clusters and dispersed DPPC molecules were recruited onto the surface of small N_2 gas nanobubbles within a few ns. Then, lipid-coated N_2 gas nanobubbles could fuse into an integral lipid nanobubble in tens of ns. Finally, the self-assembled DPPC nanobubble could maintain the stable spherical structure in bulk water for the remaining time of 3 μs coarse-grained MD simulations. It is worth mention that insufficient or excessive DPPC molecules can induce lipid nanobubbles of semi-coating or tubular shape correspondingly (**Table S6**), which is consistent with the principles for self-assembly of lipids[36]. In other words, our Martini-compatible coarse-grained model of N_2 gas molecules could properly reproduce the self-assembly process of the lipid nanobubble formation, which further validated the application feasibility of our N_2 gas coarse-grained model in lipid-related biological systems.

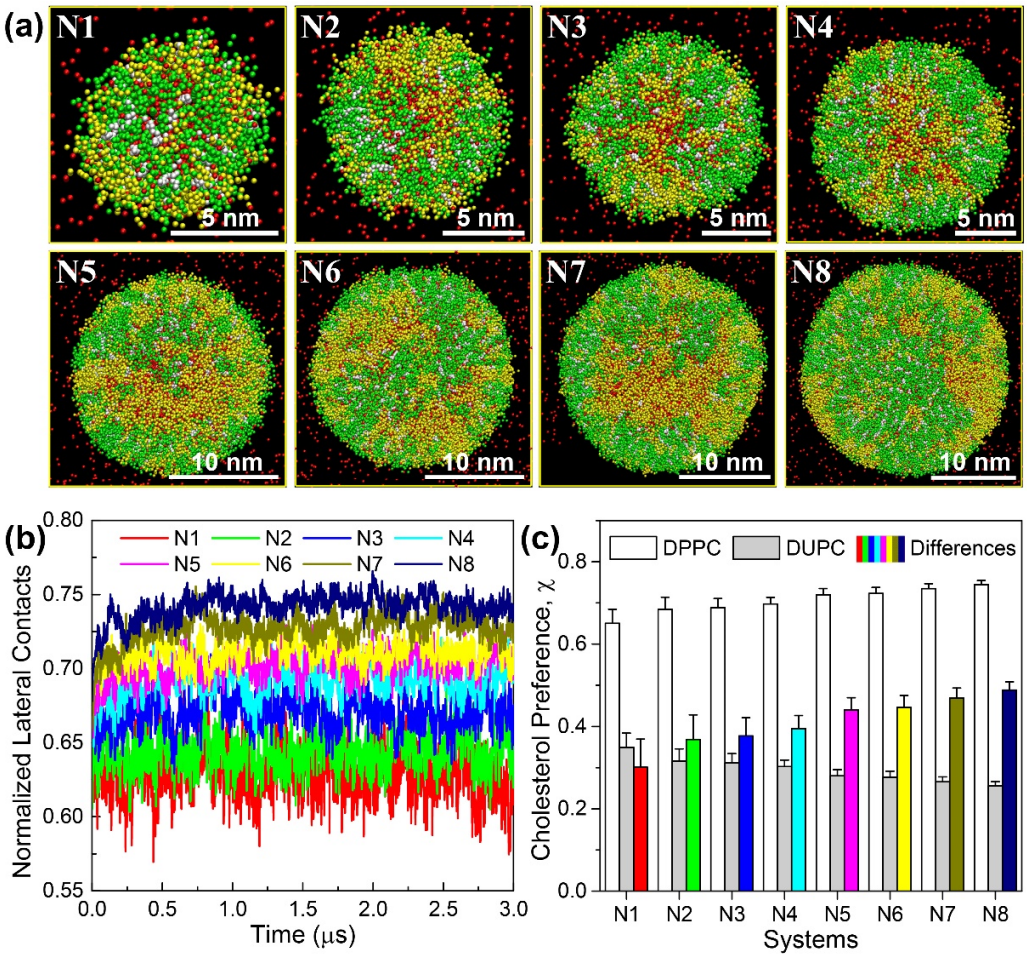

Figure 4. (a) Last frame snapshots of 3 μs MD simulations for three-component (DPPC/DUPC/Chol) lipid nanobubbles with increasing inner radius (system N1-N8, inner radius: 3-10 nm, **Table S7**). DPPC: Green; DUPC: Yellow; Chol: White; Nitrogen: Red. Water is not displayed here. All snapshots are rendered by VMD[29]. **(b)** Normalized lateral contacts of unsaturated lipids (DUPC) for system N1-N8. **(c)** Cholesterol preference to different lipids for system N1-N8.

Lipid Nanobubble and Bi-Monolayer Simulations Indicated the Critical Role of Membrane Curvature in Membrane Phase Separation. The generation of membrane curvature, which can be mediated by lipids, proteins or external stimulus, is necessary in a series of important biological processes for the proper functions of cells such as protein sorting, membrane fusion, organelle shaping and enzyme activation.[39] The presence of local membrane curvature could induce lipid sorting or redistribution [40-42], which would change the local membrane properties to fulfill certain functions. On the other hand, lipid rafts, which are driven by liquid-liquid phase separation of membrane lipids and proteins, also play critical roles in membrane-related biological processes. However, whether and how membrane curvature modulates the size and stability of lipid rafts is still unclear. As discussed above, the spherical lipid nanobubble, which has only one lipid leaflet, may serve as an ideal model system for this purpose. Hence, we set up 8 three-component lipid

nanobubble systems (system N1-N8) containing DPPC, DUPC and CHOL molecules with the initial inner nanobubble radius ranging from 3 nm to 10 nm. The system details could be found in **Table S7**. As shown in **Fig. 4a**, obvious membrane phase separation appeared in our lipid nanobubbles, which is similar to the cases of lipid vesicles[43-44]. Larger lipid nanobubbles (smaller membrane curvature) would have more obvious membrane phase separation, which was further validated by quantifying the normalized lateral contacts of unsaturated lipids (**Fig. 4b**) as well as cholesterol preferences (**Fig. 4c**). As is known, for the phase separated lipid bilayer system, membrane domains have both the *intra-leaflet*[43, 45-47] and *inter-leaflet*[48-54] dynamics. Usually, these two kinds of membrane domain dynamics are closely related to each other. In other words, our lipid nanobubbles allow the investigation of effects of membrane curvature on *intra-leaflet* membrane domain dynamics exclusively.

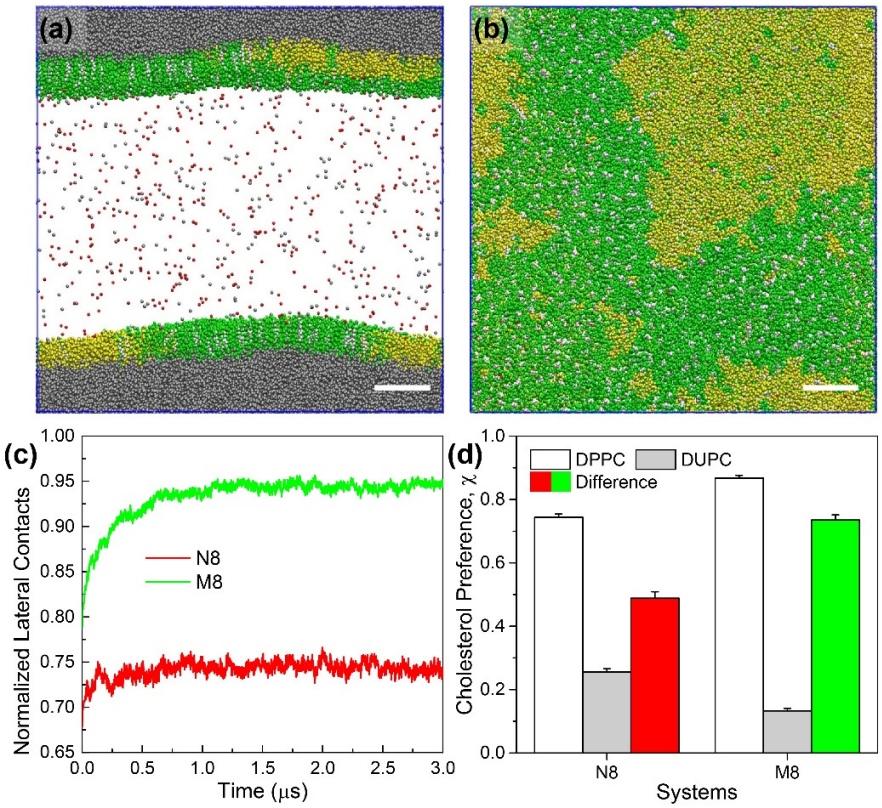

Figure 5. **(a)** Side-view and **(b)** top-view system snapshots of the lipid bi-monolayer simulation at t=3 μs (system M8, **Table S8**). DPPC is colored in green, DUPC in yellow, CHOL in white, water in gray and N_2 in red. **(c)** Normalized lateral contacts of unsaturated lipids for system N8 and M8. **(d)** Cholesterol preference to DPPC, DUPC and their differences for system N8 and M8.

As the radius of the lipid nanobubble increases, MD simulations need much more computational resources. Hence, the largest lipid nanobubble we investigated in this work only has the inner radius of 10 nm. In order to make up this shortcoming, we set up the planar lipid bi-monolayer systems (**Fig. 5a-b**) to simulate the case with the radius $\rightarrow \infty$. System M8 (**Table S8**) has the same number of lipids and area per lipid in each monolayer as that of system N8. As shown in **Fig. 5c-d**, the

results clearly indicated that system M8 had much more obvious membrane phase separation than that of system N8, which further validated the point that the degree of membrane phase separation decreased with the degree of membrane curvature (reciprocal of radius of the curvature). It is worth mention that N_2 gas molecules were introduced into our lipid bi-monolayer simulations to directly model gas phase, which was widely modeled by the vaccum in previous state-of-art coarse-grained MD simulations of lung surfactant [22, 55-58]. When the vacuum is used, the z-compressibility of the simulation box has to be zero. With the real gas molecules in the simulations, this setup is no longer necessary. Besides, the explicit interactions between gas molecules and lipids may facilitate the better description of the dynamics of interfacial lung surfactant lipids during the exhalation (monolayer compression) and inhalation (monolayer expansion) processes.

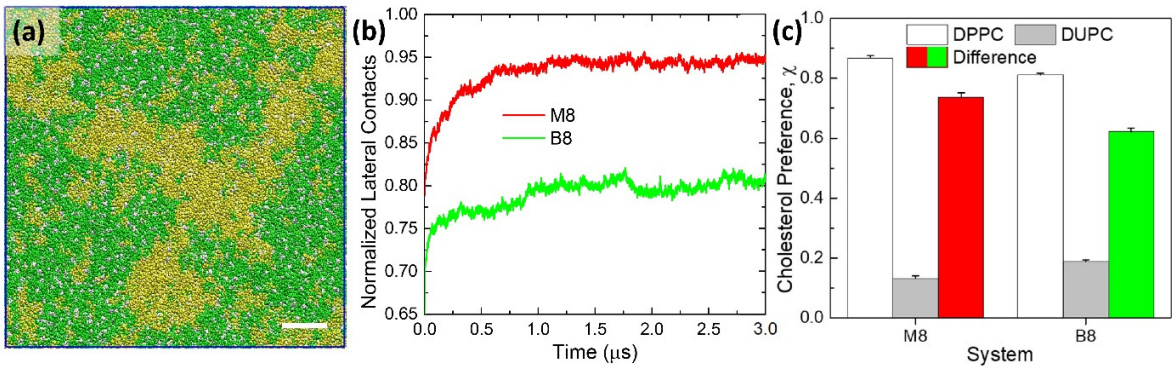

Figure 6. **(a)** Top-view system snapshot of the lipid bilayer simulation at t=3 μs (system B8, **Table S9**). DPPC is colored in green, DUPC in yellow, and CHOL in white. **(b)** Normalized lateral contacts of unsaturated lipids for system B8 and M8. **(c)** Cholesterol preference to DPPC, DUPC and their differences for system B8 and M8.

Lipid Bi-Monolayer and Bilayer Simulations Demonstrated Inter-leaflet Couplings Modulate the Membrane Phase Separation. As is discussed above, in the absence of *inter-leaflet* couplings, obvious membrane phase separation appears in both lipid nanobubble and bi-monolayer systems. Previous studies have indicated that *inter-leaflet* couplings, which can be regulated by many physicochemical factors[54], modulate membrane domain registration/anti-registration dynamics [48-50]. Whether *inter-leaflet* couplings can affect the *intra-leaflet* membrane domain dynamics is still not clear. Here, lipid bi-monolayer and bilayer systems with the same lipid number and comparable area per lipid will allow us to resolve this question directly. As shown in **Fig. 6**, compared to the lipid bilayer system (system B8, **Table S9**), lipid bi-monolayer system (system M8, **Table S8**) has much more obvious membrane phase separation. In other words, the *inter-leaflet* couplings may inhibit the *intra-leaflet* membrane domain dynamics in our simulation systems.

Conclusions

In this work, based on the density of N_2 gas molecules[24] as well as previous atomistic MD simulations of N_2 gas nanobubbles[23] and N_2-lipid bilayer systems[12], we obtained Martini-

compatible coarse-grained N_2 gas model through a series of benchmark simulations, which defined the detailed LJ nonbonded interaction parameters between N_2 and other molecules (**Table 1**). The subsequent lipid nanobubble self-assembly simulations further validated the feasibility of our coarse-grained N_2 gas model. Hence, we applied this model to study the lipid dynamics of three-component lipid nanobubbles. The results indicate that the mixture of saturated and unsaturated lipids as well as cholesterol can go through a clear phase separation in lipid nanobubbles. The larger the lipid nanobubble size, the more obvious the membrane phase separation will be. The lipid bi-monolayer simulations further confirmed the role of membrane curvature in the phase separation of single membrane leaflet. It also showed the feasibility of our gas model for pulmonary surfactant simulations, which may overcome the possible artefacts of using vacuum for the gas phase in previous coarse-grained MD simulations [22, 55-58]. Besides, by comparing lipid bi-monolayer and bilayer simulations, our results indicated that *inter-leaflet* coupling could hinder the *intra-leaflet* membrane domain dynamics. In short, our work shows that the developed coarse-grained N_2 gas model can be well applied to simulate lipid nanobubbles with complex lipid components and thus related gas-water interface, which are essential for studying the interaction molecular mechanism between lipid nanobubbles and biological systems. However, further efforts are urgently needed to develop coarse-grained models of other common gas molecules for lipid nanobubbles and explore the interactions between lipid nanobubbles (may include proteins and encapsulated drug molecules) and biological systems, which are essential for promoting the wider biomedical applications of lipid nanobubbles.

Acknowledgments

This work was supported by the National Natural Science Foundation of China (*No*. 21903002), the Fundamental Research Funds for the Central Universities (*No*. YWF-20-BJ-J-632), and the Open Fund of State Key Laboratory of Membrane Biology (No. 2020KF09). We are grateful to Center for High Performance Computing of Beihang University (BHHPC) for generous computing resources.

References

[1] Michailidi, E. D.; Bomis, G.; Varoutoglou, A.; Kyzas, G. Z.; Mitrikas, G.; Mitropoulos, A. C.; Efthimiadou, E. K.; Favvas, E. P. Bulk Nanobubbles: Production and Investigation of Their Formation/Stability Mechanism. *J. Colloid Interface Sci.* **2020**, *564*, 371-380.

[2] Nirmalkar, N.; Pacek, A. W.; Barigou, M. On the Existence and Stability of Bulk Nanobubbles. *Langmuir* **2018**, *34*, 10964-10973.

[3] Liu, R.; Tang, J.; Xu, Y.; Dai, Z. Bioluminescence Imaging of Inflammation in Vivo Based on Bioluminescence and Fluorescence Resonance Energy Transfer Using Nanobubble Ultrasound Contrast Agent. *ACS Nano* **2019**, *13*, 5124-5132.

[4] Fang, K.; Wang, L.; Huang, H.; Lan, M.; Shen, D.; Dong, S.; Guo, Y. Construction of Nucleolin-Targeted Lipid Nanobubbles and Contrast-Enhanced Ultrasound Molecular Imaging in Triple-Negative Breast Cancer. *Pharm. Res.* **2020**, *37*, 145.

[5] Batchelor, D. V. B.; Abou-Saleh, R. H.; Coletta, P. L.; McLaughlan, J. R.; Peyman, S. A.; Evans, S. D. Nested Nanobubbles for Ultrasound-Triggered Drug Release. *ACS Appl. Mater. Interfaces* **2020**, *12*, 29085-29093.

[6] Zhu, Y.; Zhang, G.; Li, M.; Ma, L.; Huang, J.; Qiu, L. Ultrasound-Augmented Phase Transition Nanobubbles for Targeted Treatment of Paclitaxel-Resistant Cancer. *Bioconjugate Chem.* **2020**, *31*, 2008-2020.

[7] Atkinson, A. J.; Apul, O. G.; Schneider, O.; Garcia-Segura, S.; Westerhoff, P. Nanobubble Technologies Offer Opportunities to Improve Water Treatment. *Acc. Chem. Res.* **2019**, *52*, 1196-1205.

[8] Agarwal, A.; Ng, W. J.; Liu, Y. Principle and Applications of Microbubble and Nanobubble Technology for Water Treatment. *Chemosphere* **2011**, *84*, 1175-1180.

[9] Um, W., et al. Necroptosis-Inducible Polymeric Nanobubbles for Enhanced Cancer Sonoimmunotherapy. *Adv. Mater.* **2020**, *32*, 1907953.

[10] Zuo, Y. Y.; Veldhuizen, R. A. W.; Neumann, A. W.; Petersen, N. O.; Possmayer, F. Current Perspectives in Pulmonary Surfactant — Inhibition, Enhancement and Evaluation. *Biochim. Biophys. Acta-Biomembr.* **2008**, *1778*, 1947-1977.

[11] Sun, D.; Lin, X.; Zhang, Z.; Gu, N. Impact of Shock-Induced Lipid Nanobubble Collapse on a Phospholipid Membrane. *J. Phys. Chem. C* **2016**, *120*, 18803-18810.

[12] Li, J.; Zhang, X.; Cao, D. Decoupling of Bilayer Leaflets under Gas Supersaturation: Nitrogen Nanobubbles in a Membrane and Their Implication in Decompression Sickness. *J. Phys. D: Appl. Phys.* **2018**, *51*, 184001.

[13] Karplus, M.; McCammon, J. A. Molecular Dynamics Simulations of Biomolecules. *Nat. Struct. Biol.* **2002**, *9*, 646-652.

[14] Goliaei, A.; Adhikari, U.; Berkowitz, M. L. Opening of the Blood-Brain Barrier Tight Junction Due to Shock Wave Induced Bubble Collapse: A Molecular Dynamics Simulation Study. *ACS Chem. Neurosci.* **2015**, *6*, 1296-1301.

[15] Venable, R. M.; Krämer, A.; Pastor, R. W. Molecular Dynamics Simulations of Membrane Permeability. *Chem. Rev.* **2019**, *119*, 5954-5997.

[16] Lu, X.-M.; Yuan, B.; Zhang, X.-R.; Yang, K.; Ma, Y.-Q. Molecular Modeling of Transmembrane Delivery of Paclitaxel by Shock Waves with Nanobubbles. *Appl. Phys. Lett.* **2017**, *110*, 023701.

[17] Marrink, S. J.; Risselada, H. J.; Yefimov, S.; Tieleman, D. P.; de Vries, A. H. The Martini Force Field: Coarse Grained Model for Biomolecular Simulations. *J. Phys. Chem. B* **2007**, *111*, 7812-7824.

[18] Monticelli, L.; Kandasamy, S. K.; Periole, X.; Larson, R. G.; Tieleman, D. P.; Marrink, S.-J. The Martini Coarse-Grained Force Field: Extension to Proteins. *J. Chem. Theory Comput.* **2008**, *4*, 819-834.

[19] Marrink, S. J.; Tieleman, D. P. Perspective on the Martini Model. *Chem. Soc. Rev.* **2013**, *42*, 6801-6822.

[20] Min, S. H.; Wijesinghe, S.; Lau, E. Y.; Berkowitz, M. L. Damage to Polystyrene Polymer Film by Shock Wave Induced Bubble Collapse. *J. Phys. Chem. B* **2020**, *124*, 7494-7499.

[21] Luo, Z.; Li, S.; Xu, Y.; Yan, Z.; Huang, F.; Yue, T. The Role of Nanoparticle Shape in Translocation across the Pulmonary Surfactant Layer Revealed by Molecular Dynamics Simulations. *Environ. Sci.: Nano* **2018**, *5*, 1921-1932.

[22] Tian, F.; Lin, X.; Valle, R. P.; Zuo, Y. Y.; Gu, N. Poly(Amidoamine) Dendrimer as a Respiratory Nanocarrier: Insights from Experiments and Molecular Dynamics Simulations. *Langmuir* **2019**, *35*, 5364-5371.
[23] Zhang, M.; Tu, Y.-s.; Fang, H.-p. Concentration of Nitrogen Molecules Needed by Nitrogen Nanobubbles Existing in Bulk Water. *Appl. Math. Mech. -Engl. Ed.* **2013**, *34*, 1433-1438.
[24] Engineering Toolbox. Nitrogen - Density and Specific Weight [Online]. **2018**, Available at: https://www.engineeringtoolbox.com/nitrogen-N2-density-specific-weight-temperature-pressure-d_2039.html [Accessed 15 Dec. 2020].
[25] Zhou, L., et al. Ultrahigh Density of Gas Molecules Confined in Surface Nanobubbles in Ambient Water. *J. Am. Chem. Soc.* **2020**, *142*, 5583-5593.
[26] Cwiklik, L. Tear Film Lipid Layer: A Molecular Level View. *Biochim. Biophys. Acta-Biomembr.* **2016**, *1858*, 2421-2430.
[27] Krupka, T. M.; Solorio, L.; Wilson, R. E.; Wu, H.; Azar, N.; Exner, A. A. Formulation and Characterization of Echogenic Lipid-Pluronic Nanobubbles. *Mol. Pharm.* **2010**, *7*, 49-59.
[28] Abraham, M. J.; Murtola, T.; Schulz, R.; Páll, S.; Smith, J. C.; Hess, B.; Lindahl, E. Gromacs: High Performance Molecular Simulations through Multi-Level Parallelism from Laptops to Supercomputers. *SoftwareX* **2015**, *1-2*, 19-25.
[29] Humphrey, W.; Dalke, A.; Schulten, K. Vmd: Visual Molecular Dynamics. *J. Mol. Graph.* **1996**, *14*, 33-38.
[30] Bussi, G.; Donadio, D.; Parrinello, M. Canonical Sampling through Velocity Rescaling. *J. Chem. Phys.* **2007**, *126*, 014101.
[31] Parrinello, M.; Rahman, A. Polymorphic Transitions in Single Crystals: A New Molecular Dynamics Method. *J. Appl. Phys.* **1981**, *52*, 7182-7190.
[32] Cao, F.; Deetz, J. D.; Sun, H. Free Energy-Based Coarse-Grained Force Field for Binary Mixtures of Hydrocarbons, Nitrogen, Oxygen, and Carbon Dioxide. *J. Chem. Inf. Model.* **2017**, *57*, 50-59.
[33] Sever, N.; Miličić, G.; Bodnar, N. O.; Wu, X.; Rapoport, T. A. Mechanism of Lamellar Body Formation by Lung Surfactant Protein B. *Mol. Cell* **2020**, doi: 10.1016/j.molcel.2020.10.042.
[34] Tian, J.; Yang, F.; Cui, H.; Zhou, Y.; Ruan, X.; Gu, N. A Novel Approach to Making the Gas-Filled Liposome Real: Based on the Interaction of Lipid with Free Nanobubble within the Solution. *ACS Appl. Mater. Interfaces* **2015**, *7*, 26579-84.
[35] Zheng, R.; Yin, T.; Wang, P.; Zheng, R.; Zheng, B.; Cheng, D.; Zhang, X.; Shuai, X.-T. Nanobubbles for Enhanced Ultrasound Imaging of Tumors. *Int. J. Nanomed.* **2012**, *7*, 895-904.
[36] Antonietti, M.; Förster, S. Vesicles and Liposomes: A Self-Assembly Principle Beyond Lipids. *Adv. Mater.* **2003**, *15*, 1323-1333.
[37] Yang, G.; O'Duill, M.; Gouverneur, V.; Krafft, M. P. Recruitment and Immobilization of a Fluorinated Biomarker across an Interfacial Phospholipid Film Using a Fluorocarbon Gas. *Angew. Chem. Int. Ed. Engl.* **2015**, *54*, 8402-8406.
[38] Brea, R. J.; Cole, C. M.; Devaraj, N. K. In Situ Vesicle Formation by Native Chemical Ligation. *Angew. Chem. Int. Ed. Engl.* **2014**, *53*, 14102-14105.
[39] McMahon, H. T.; Boucrot, E. Membrane Curvature at a Glance. *J. Cell Sci.* **2015**, *128*, 1065-1070.
[40] Beltrán-Heredia, E.; Tsai, F.-C.; Salinas-Almaguer, S.; Cao, F. J.; Bassereau, P.; Monroy, F. Membrane

Curvature Induces Cardiolipin Sorting. *Commun. Biol.* **2019**, *2*, 225.
[41] Lin, X.; Wang, H.; Lou, Z.; Cao, M.; Zhang, Z.; Gu, N. Roles of Pip2 in the Membrane Binding of Mim I-Bar: Insights from Molecular Dynamics Simulations. *FEBS Lett.* **2018**, *592*, 2533-2542.
[42] Baoukina, S.; Ingólfsson, H. I.; Marrink, S. J.; Tieleman, D. P. Curvature-Induced Sorting of Lipids in Plasma Membrane Tethers. *Adv. Theory Simul.* **2018**, *1*, 1800034.
[43] Risselada, H. J.; Marrink, S. J. The Molecular Face of Lipid Rafts in Model Membranes. *Proc. Natl. Acad. Sci. U. S. A.* **2008**, *105*, 17367-17372.
[44] Kaiser, H.-J.; Lingwood, D.; Levental, I.; Sampaio, J. L.; Kalvodova, L.; Rajendran, L.; Simons, K. Order of Lipid Phases in Model and Plasma Membranes. *Proc. Natl. Acad. Sci. U. S. A.* **2009**, *106*, 16645-16650.
[45] Lin, X.; Lorent, J. H.; Skinkle, A. D.; Levental, K. R.; Waxham, M. N.; Gorfe, A. A.; Levental, I. Domain Stability in Biomimetic Membranes Driven by Lipid Polyunsaturation. *J. Phys. Chem. B* **2016**, *120*, 11930-11941.
[46] Gu, R.-X.; Baoukina, S.; Tieleman, D. P. Phase Separation in Atomistic Simulations of Model Membranes. *J. Am. Chem. Soc.* **2020**, *142*, 2844-2856.
[47] Heberle, F. A.; Feigenson, G. W. J. C. S. H. p. i. b. Phase Separation in Lipid Membranes. *Cold Spring Harb. Perspect. Biol.* **2011**, *3*, a004630.
[48] Lin, X.; Zhang, S.; Ding, H.; Levental, I.; Gorfe, A. A. The Aliphatic Chain of Cholesterol Modulates Bilayer Interleaflet Coupling and Domain Registration. *FEBS Lett.* **2016**, *590*, 3368-3374.
[49] Zhang, S.; Lin, X. Lipid Acyl Chain Cis Double Bond Position Modulates Membrane Domain Registration/Anti-Registration. *J. Am. Chem. Soc.* **2019**, *141*, 15884-15890.
[50] Fowler, P. W.; Williamson, J. J.; Sansom, M. S. P.; Olmsted, P. D. Roles of Interleaflet Coupling and Hydrophobic Mismatch in Lipid Membrane Phase-Separation Kinetics. *J. Am. Chem. Soc.* **2016**, *138*, 11633-11642.
[51] Seo, S.; Murata, M.; Shinoda, W. Pivotal Role of Interdigitation in Interleaflet Interactions: Implications from Molecular Dynamics Simulations. *J. Phys. Chem. Lett.* **2020**, *11*, 5171-5176.
[52] Thallmair, S.; Ingólfsson, H. I.; Marrink, S. J. Cholesterol Flip-Flop Impacts Domain Registration in Plasma Membrane Models. *J. Phys. Chem. Lett.* **2018**, *9*, 5527-5533.
[53]Perlmutter, J. D.; Sachs, J. N. Interleaflet Interaction and Asymmetry in Phase Separated Lipid Bilayers: Molecular Dynamics Simulations. *J. Am. Chem. Soc.* **2011**, *133*, 6563-6577.
[54] Nickels, J. D.; Smith, J. C.; Cheng, X. Lateral Organization, Bilayer Asymmetry, and Inter-Leaflet Coupling of Biological Membranes. *Chem. Phys. Lipids* **2015**, *192*, 87-99.
[55] Hu, G.; Jiao, B.; Shi, X.; Valle, R. P.; Fan, Q.; Zuo, Y. Y. Physicochemical Properties of Nanoparticles Regulate Translocation across Pulmonary Surfactant Monolayer and Formation of Lipoprotein Corona. *ACS Nano* **2013**, *7*, 10525-10533.
[56] Bai, X.; Li, M.; Hu, G. Nanoparticle Translocation across the Lung Surfactant Film Regulated by Grafting Polymers. *Nanoscale* **2020**, *12*, 3931-3940.
[57] Xu, Y.; Li, S.; Luo, Z.; Ren, H.; Zhang, X.; Huang, F.; Zuo, Y. Y.; Yue, T. Role of Lipid Coating in the Transport of Nanodroplets across the Pulmonary Surfactant Layer Revealed by Molecular Dynamics Simulations. *Langmuir* **2018**, *34*, 9054-9063.
[58] Baoukina, S.; Mendez-Villuendas, E.; Tieleman, D. P. Molecular View of Phase Coexistence in Lipid

Monolayers. *J. Am. Chem. Soc.* **2012**, *134*, 17543-17553.

Supporting Information for

Developing Martini Coarse-Grained Nitrogen Gas Model for Lipid Nanobubble Simulations

Fujia Tian[1,2,#], Xubo Lin[1,#,*]

1. Institute of Single Cell Engineering, Key Laboratory of Ministry of Education for Biomechanics and Mechanobiology, Beijing Advanced Innovation Center for Biomedical Engineering, School of Biological Science and Medical Engineering, Beihang University, Beijing 100191, China.
2. Current Affiliation: Department of Physics, City University of Hong Kong, Hong Kong 999077, China.

* Correspondence to: linxbseu@buaa.edu.cn (XL).
# These authors contribute equally to this work.
The authors declare no competing financial interest.

Table S1. Lennar-Jones (LJ) interaction Matrix in Martini model. Energy parameters (ε kJ/mol) summarized from the work of Marrink *et al*.[1]

	C1	C2	C3	C4	C5	N0	Na	Nd	Nda	P1	P2	P3	P4	P5	Q0	Qa	Qd	Qda
C1	3.5	3.5	3.5	3.1	3.1	2.7	2.7	2.7	2.7	2.7	2.3	2.3	2.0	2.0	2.0	2.0	2.0	2.0
C2		3.5	3.5	3.1	3.1	3.1	2.7	2.7	2.7	3.1	2.7	2.7	2.3	2.3	2.0	2.0	2.0	2.0
C3			3.5	3.5	3.5	3.5	2.7	2.7	2.7	3.5	3.1	3.1	2.7	2.7	2.3	2.3	2.3	2.3
C4				3.5	3.5	3.5	3.1	3.1	3.1	3.5	3.5	3.1	2.7	2.7	2.7	2.7	2.7	2.7
C5					3.5	3.5	3.5	3.5	3.5	3.5	3.5	3.5	3.1	3.1	3.1	3.1	3.1	3.1
N0						3.5	3.5	3.5	3.5	4.0	4.0	3.5	3.5	3.5	3.5	3.5	3.5	3.5
Na							4.0	4.5	4.5	4.5	4.5	4.5	4.0	5.0	4.0	4.0	5.0	5.0
Nd								4.0	4.5	4.5	4.5	4.5	4.0	5.0	4.0	5.0	4.0	5.0
Nda									4.5	4.5	4.5	4.5	4.0	5.0	4.0	5.0	5.0	5.0
P1										4.5	4.5	4.5	4.5	5.6	4.0	5.0	5.0	5.0
P2											4.5	4.5	4.5	5.6	4.5	5.0	5.0	5.0
P3												5.0	5.0	5.6	5.0	5.6	5.6	5.6
P4													5.0	5.6	5.6	5.6	5.6	5.6
P5														5.6	5.0	5.6	5.6	5.6
Q0															3.5	4.5	4.5	4.5
Qa																5.0	5.6	5.6
Qd																	5.0	5.6
Qda																		5.6

σ=0.47 nm for all interaction groups except σ=0.62 nm for C1 bead interacting with charged beads (Q).

Table S2. Scaling factor and corresponding parameters in LJ potential for non-bonded interaction between nitrogen and water beads.

Number	k	σ (nm)	ε (kJ/mol)	Attractive term	Repulsive term
1	0	0.42	1.9	4.1717E-02	2.2898E-04
2	0.08	0.42	1.7	3.7325E-02	2.0488E-04
3	0.12	0.42	1.6	3.5130E-02	1.9283E-04
4	0.2	0.42	1.5	3.2934E-02	1.8078E-04
5	0.24	0.42	1.4	3.0739E-02	1.6873E-04
6	0.28	0.42	1.3	2.8543E-02	1.5667E-04

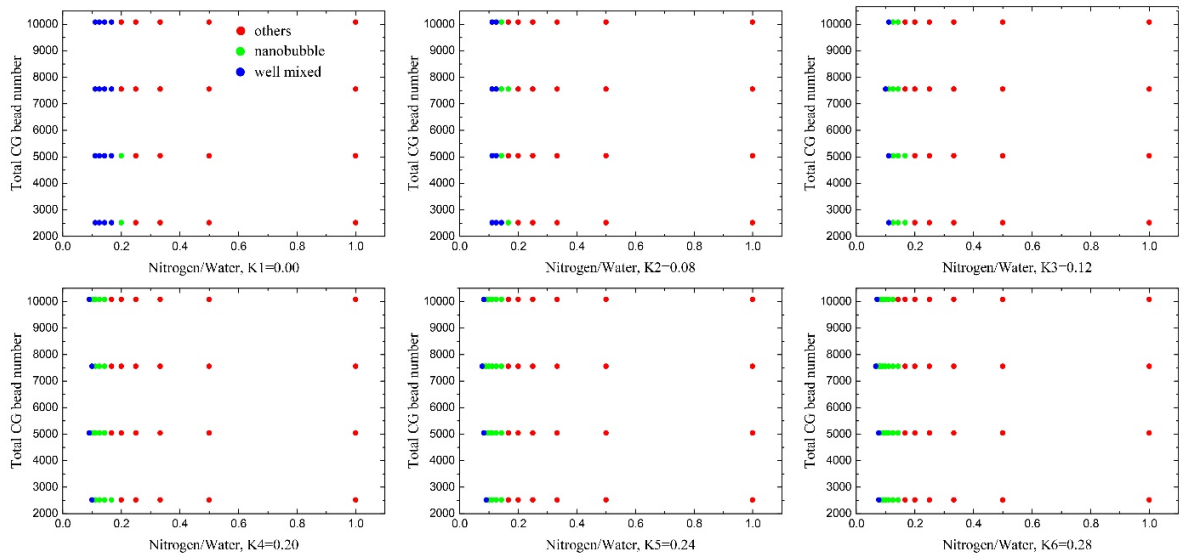

Figure S1. Coarse-grained molecular dynamics (MD) simulations of mixed systems of N_2 gas and water molecules with different scaling factors. Systems of different size and nitrogen/water ratio were investigated for each scaling factor.

Table S3. Critical concentration (g/L) for nitrogen nanobubble formation obtained from simulations of nitrogen-water mixtures with different LJ interaction parameter combinations.

	G1-G1 (σ=0.36 nm)													
	ε (kJ/mol)	0.7	0.8	0.9	1.0	1.1	1.2	1.3	1.4	1.5	1.6	1.7	1.8	1.9
	1.1	22	22	22	20	20	20	18	18	18	16	14	14	14
	1.2	24	22	24	24	22	20	20	18	18	16	16	16	14
	1.3	26	28	26	26	24	24	22	20	20	18	18	16	16
G1-P4	1.4	>30	30	30	30	30	28	26	24	24	22	20	20	18
(σ=0.42	1.5	>30	>30	>30	>30	30	>30	30	28	28	26	24	24	20
nm)	1.6	>30	>30	>30	>30	>30	>30	>30	>30	>30	30	26	26	24
	1.7	>30	>30	>30	>30	>30	>30	>30	>30	>30	>30	>30	30	26
	1.8	>30	>30	>30	>30	>30	>30	>30	>30	>30	>30	>30	>30	>30
	1.9	>30	>30	>30	>30	>30	>30	>30	>30	>30	>30	>30	>30	>30
	2.0	>30	>30	>30	>30	>30	>30	>30	>30	>30	>30	>30	>30	>30

Table S4. Configurations of initial simulation systems for determining critical concentration of N_2 nanobubble formation.

Number	N_2 **Conc.(g/L)**	***No.* of N_2**	***No.* of water**
1	10.0	85	3290
2	12.0	101	3274
3	14.0	117	3258
4	16.0	133	3242

5	18.0	149	3226
6	20.0	165	3210
7	22.0	181	3194
8	24.0	196	3179
9	26.0	211	3164
10	28.0	227	3148
11	30.0	242	3133

Table S5. Benchmark setups for determining LJ parameters of G1-Na and G1-C1 non-bonded interactions.

Group 1				
Cross-term		**ε (kJ/mol)**	**Attractive term**	**Repulsive term**
G1-G1 (σ=0.36 nm)		1.6	1.3931E-02	3.0326E-05
G1-P4 (σ=0.42 nm)		1.4	3.0739E-02	1.6873E-04
G1-Q0 (σ=0.49 nm)		1.4	7.7511E-02	1.0729E-03
G1-Qa (σ=0.49 nm)		1.4	7.7511E-02	1.0729E-03
G1-C1 (σ=0.42 nm)		1.6	3.5130E-02	1.9283E-04
G1-Na (σ=0.42 nm)	a	1.4	3.0739E-02	1.6873E-04
	b	1.5	3.2934E-02	1.8078E-04
	c	1.6	3.5130E-02	1.9283E-04

Group 2				
Cross-term		**ε (kJ/mol)**	**Attractive term**	**Repulsive term**
G1-G1 (σ=0.36 nm)		1.6	1.3931E-02	3.0326E-05
G1-P4 (σ=0.42 nm)		1.4	3.0739E-02	1.6873E-04
G1-Q0 (σ=0.49 nm)		1.4	7.7511E-02	1.0729E-03
G1-Qa (σ=0.49 nm)		1.4	7.7511E-02	1.0729E-03
G1-C1 (σ=0.42 nm)		1.7	3.7325E-02	2.0488E-04
G1-Na (σ=0.42 nm)	a	1.4	3.0739E-02	1.6873E-04
	b	1.5	3.2934E-02	1.8078E-04
	c	1.6	3.5130E-02	1.9283E-04
	d	1.7	3.7325E-02	2.0488E-04

Group 3			
Cross-term	**ε (kJ/mol)**	**Attractive term**	**Repulsive term**
G1-G1 (σ=0.36 nm)	1.6	1.3931E-02	3.0326E-05
G1-P4 (σ=0.42 nm)	1.4	3.0739E-02	1.6873E-04
G1-Q0 (σ=0.49 nm)	1.4	7.7511E-02	1.0729E-03
G1-Qa (σ=0.49 nm)	1.4	7.7511E-02	1.0729E-03
G1-C1 (σ=0.42 nm)	1.8	3.9521E-02	2.1693E-04

G1-Na (σ=0.42 nm)	a	1.4	3.0739E-02	1.6873E-04
	b	1.5	3.2934E-02	1.8078E-04
	c	1.6	3.5130E-02	1.9283E-04
	d	1.7	3.7325E-02	2.0488E-04
	d	1.8	3.9521E-02	2.1693E-04

Group 4				
Cross-term		**ε (kJ/mol)**	**Attractive term**	**Repulsive term**
G1-G1 (σ=0.36 nm)		1.6	1.3931E-02	3.0326E-05
G1-P4 (σ=0.42 nm)		1.4	3.0739E-02	1.6873E-04
G1-Q0 (σ=0.49 nm)		1.4	7.7511E-02	1.0729E-03
G1-Qa (σ=0.49 nm)		1.4	7.7511E-02	1.0729E-03
G1-C1 (σ=0.42 nm)		1.9	4.1717E-02	2.2898E-04
G1-Na (σ=0.42 nm)	a	1.4	3.0739E-02	1.6873E-04
	b	1.5	3.2934E-02	1.8078E-04
	c	1.6	3.5130E-02	1.9283E-04
	d	1.7	3.7325E-02	2.0488E-04
	e	1.8	3.9521E-02	2.1693E-04
	f	1.9	4.1717E-02	2.2898E-04

Group 5				
Cross-term		**ε (kJ/mol)**	**Attractive term**	**Repulsive term**
G1-G1 (σ=0.36 nm)		1.6	1.3931E-02	3.0326E-05
G1-P4 (σ=0.42 nm)		1.4	3.0739E-02	1.6873E-04
G1-Q0 (σ=0.49 nm)		1.4	7.7511E-02	1.0729E-03
G1-Qa (σ=0.49 nm)		1.4	7.7511E-02	1.0729E-03
G1-C1 (σ=0.42 nm)		2.0	4.3912E-02	2.4104E-04
G1-Na (σ=0.42 nm)	a	1.4	3.0739E-02	1.6873E-04
	b	1.5	3.2934E-02	1.8078E-04
	c	1.6	3.5130E-02	1.9283E-04
	d	1.7	3.7325E-02	2.0488E-04
	e	1.8	3.9521E-02	2.1693E-04
	f	1.9	4.1717E-02	2.2898E-04
	g	2.0	4.3912E-02	2.4104E-04

Group 6			
Cross-term	**ε (kJ/mol)**	**Attractive term**	**Repulsive term**
G1-G1 (σ=0.36 nm)	1.6	1.3931E-02	3.0326E-05

G1-P4 (σ=0.42 nm)		1.4	3.0739E-02	1.6873E-04
G1-Q0 (σ=0.49 nm)		1.4	7.7511E-02	1.0729E-03
G1-Qa (σ=0.49 nm)		1.4	7.7511E-02	1.0729E-03
G1-C1 (σ=0.42 nm)		2.1	4.6108E-02	2.5309E-04
G1-Na (σ=0.42 nm)	a	1.4	3.0739E-02	1.6873E-04
	b	1.5	3.2934E-02	1.8078E-04
	c	1.6	3.5130E-02	1.9283E-04
	d	1.7	3.7325E-02	2.0488E-04
	e	1.8	3.9521E-02	2.1693E-04
	f	1.9	4.1717E-02	2.2898E-04
	g	2.0	4.3912E-02	2.4104E-04
	h	2.1	4.6108E-02	2.5309E-04

Group 7				
Cross-term		**ε (kJ/mol)**	**Attractive term**	**Repulsive term**
G1-G1 (σ=0.36 nm)		1.6	1.3931E-02	3.0326E-05
G1-P4 (σ=0.42 nm)		1.4	3.0739E-02	1.6873E-04
G1-Q0 (σ=0.49 nm)		1.4	7.7511E-02	1.0729E-03
G1-Qa (σ=0.49 nm)		1.4	7.7511E-02	1.0729E-03
G1-C1 (σ=0.42 nm)		2.2	4.8303E-02	2.6514E-04
G1-Na (σ=0.42 nm)	a	1.4	3.0739E-02	1.6873E-04
	b	1.5	3.2934E-02	1.8078E-04
	c	1.6	3.5130E-02	1.9283E-04
	d	1.7	3.7325E-02	2.0488E-04
	e	1.8	3.9521E-02	2.1693E-04
	f	1.9	4.1717E-02	2.2898E-04
	g	2.0	4.3912E-02	2.4104E-04
	h	2.1	4.6108E-02	2.5309E-04
	i	2.2	4.8303E-02	2.6514E-04

Group 1

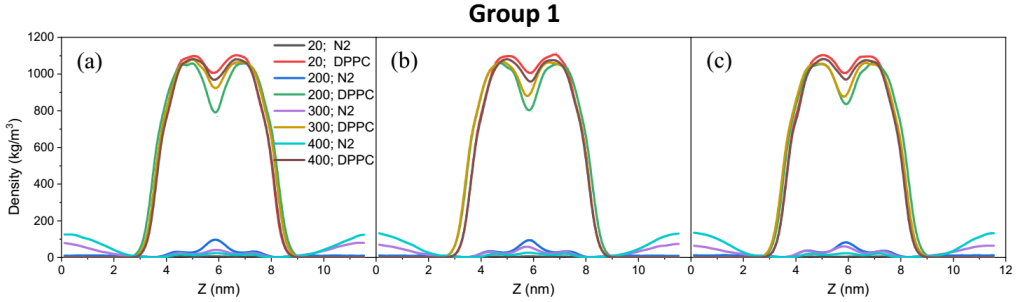

Group 2

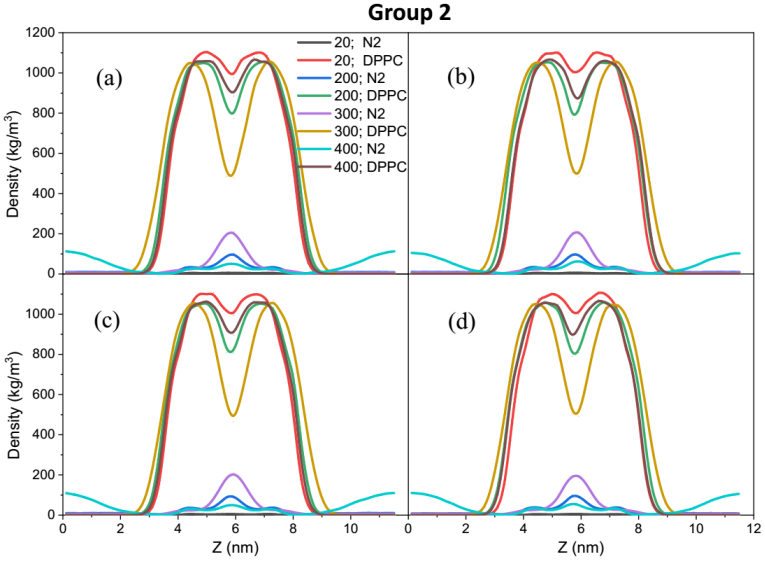

Group 3

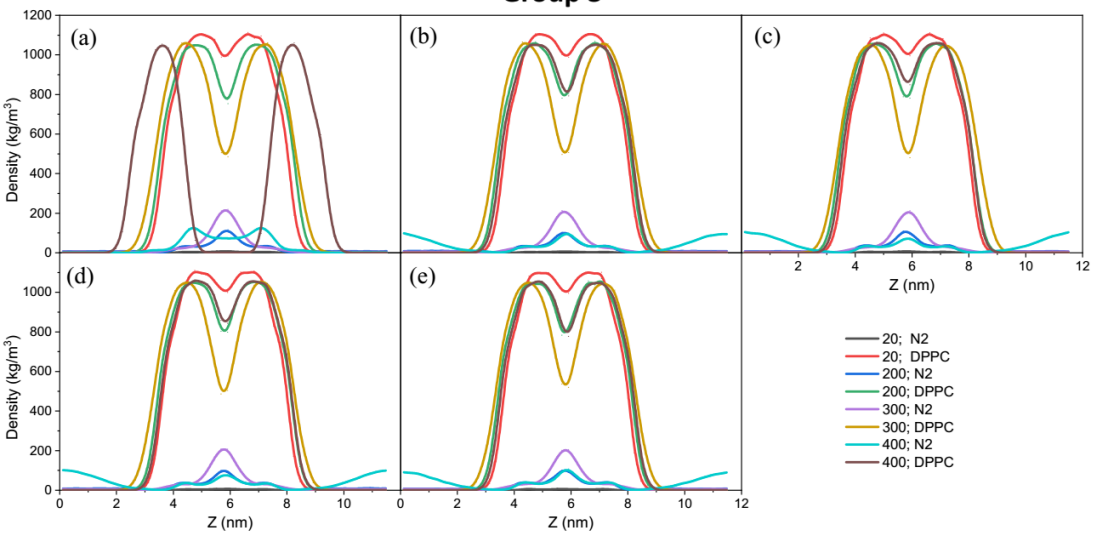

Group 4

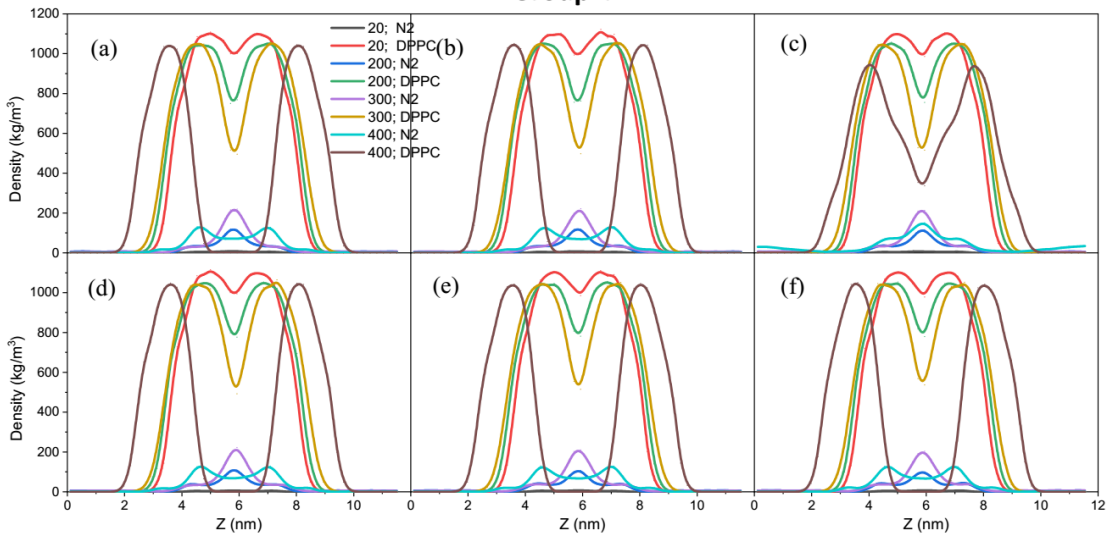

Group 5

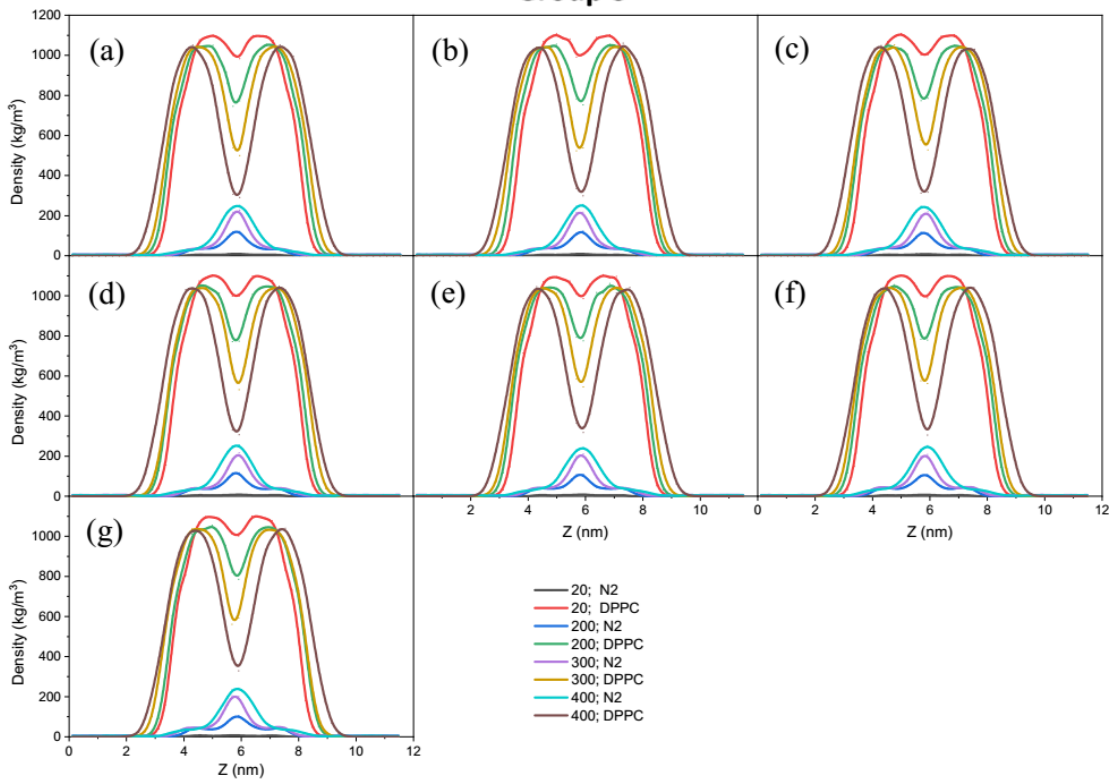

Group 6

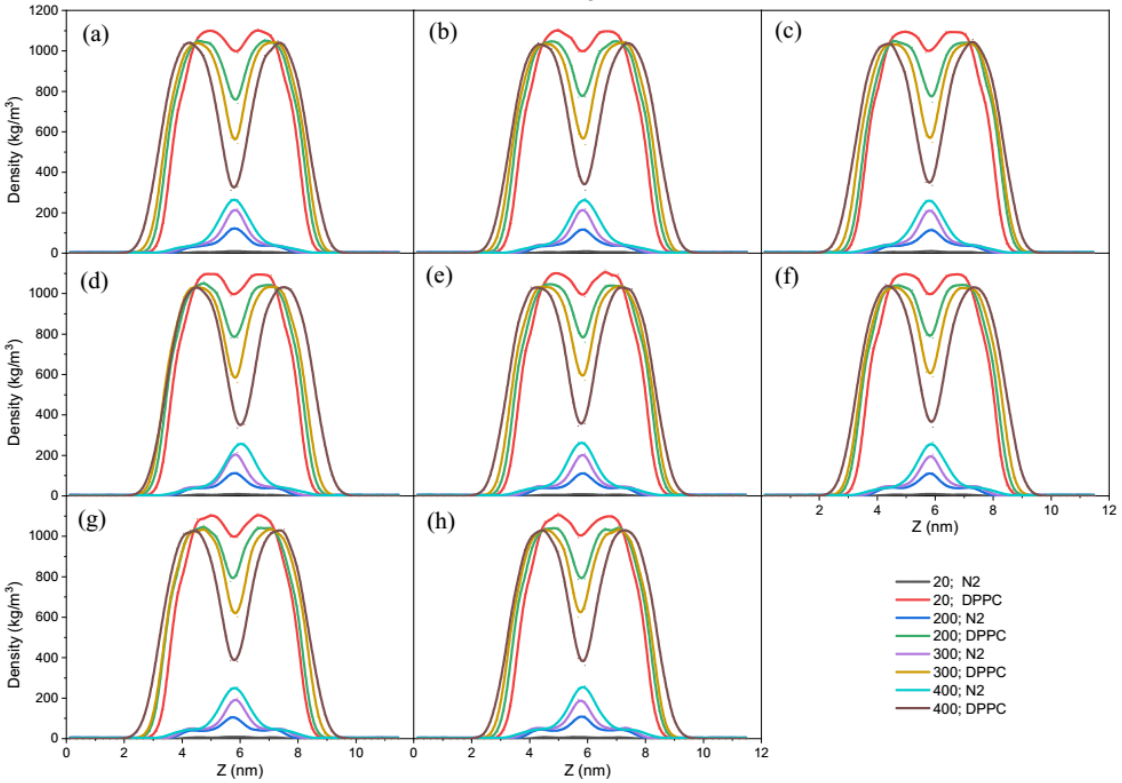

Group 7

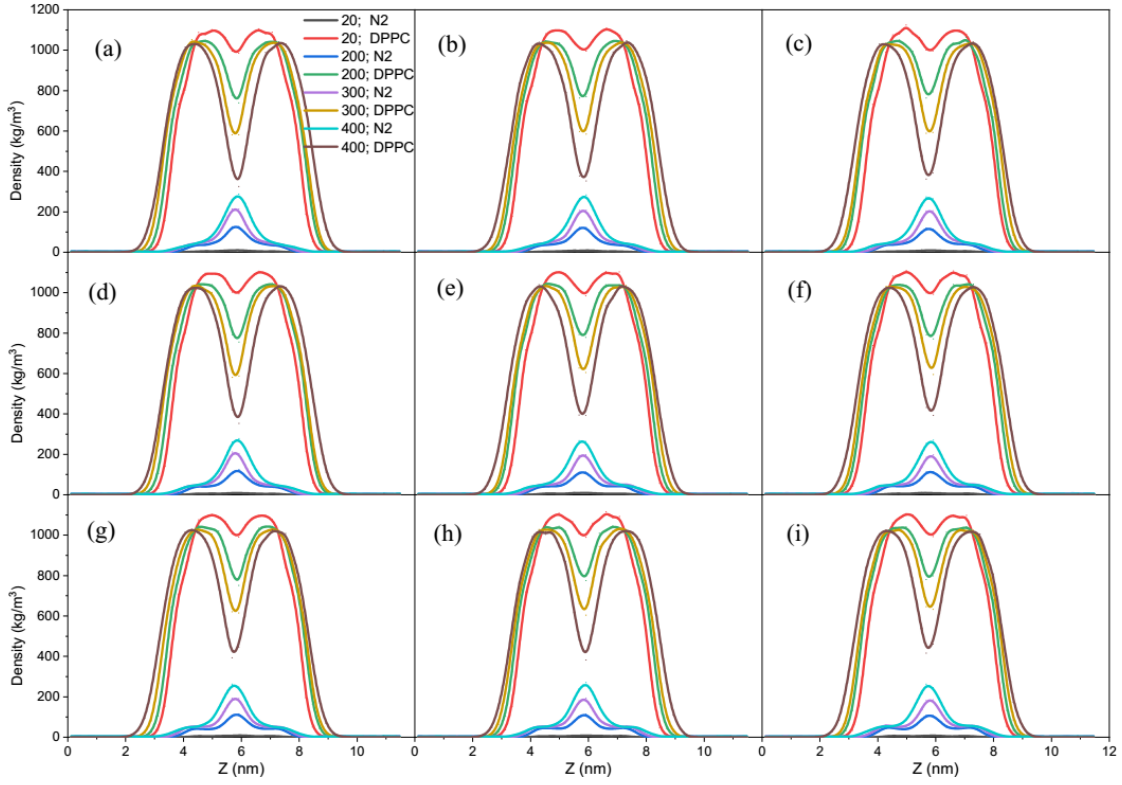

Figure S2. Density profiles of N_2 gas and DPPC molecules along the membrane normal based on G1-C1 and G1-Na interaction groups 1-7 of **Table S5**. For each LJ parameter set, four 128-DPPC bilayer systems with 20, 200, 300 or 400 N_2 gas molecules initially were evenly dispersed in bulk water region and their behaviors were investigated.

Table S6. Lipid nanobubble self-assembly simulations with different initial nitrogen nanobubble radius and different number of DPPC molecules.

System	DPPC	N_2	Radius (nm)	N_2 nanobubble ρ (g/L)	H_2O	Results
1	180	454	3	186.74	12844	Lipid nanobubble
2	180	606	3	249.26	12844	Lipid nanobubble
3	180	734	3.5	190.12	12284	Lipid nanobubble
4	180	979	3.5	253.59	12284	Lipid nanobubble
5	180	1084	4	188.10	11584	Lipid nanobubble
6	180	1446	4	250.92	11584	Semi-lipid nanobubble
7	256	438	3	180.16	13072	Tubular shape
8	256	876	3	360.32	13072	Lipid nanobubble
9	256	1091	4	189.32	11766	Lipid nanobubble
10	256	2182	4	378.63	11766	Tubular shape
11	256	1400	5	124.38	9749	Lipid nanobubble
12	256	2100	5	186.58	9749	Tubular shape

Table S7. Simulation systems of three-component lipid nanobubble.

System	DPPC	DUPC	CHOL	N_2	H_2O	N_2 Conc.(g/L)
N1	117	70	48	646	8322	30.19
N2	209	125	84	1645	19512	32.79
N3	327	196	131	2435	32027	29.57
N4	471	282	189	3431	44445	30.02
N5	641	384	257	4653	59961	30.18
N6	837	502	336	6130	78938	30.20
N7	1060	636	424	7500	99609	29.28
N8	1308	785	524	9000	120367	29.08

Table S8. Simulation system of three-component lipid bi-monolayer.

System	A (nm^2)	One leaflet			N_2	H_2O
		DPPC	DUPC	CHOL		
M8	0.64	1308	785	524	485	94136

Table S9. Simulation system of three-component lipid bilayer.

System	Outer leaflet			Inner leaflet			H_2O
	DPPC	DUPC	CHOL	DPPC	DUPC	CHOL	
B8	1308	785	524	1308	785	524	91264

References:

[1] Marrink, S. J.; Risselada, H. J.; Yefimov, S.; Tieleman, D. P.; de Vries, A. H. The Martini Force Field: Coarse Grained Model for Biomolecular Simulations. *J. Phys. Chem. B* **2007**, *111*, 7812-7824.